SAND2023-04888J

Molecular dynamics study of grain boundary and radiation effects on tritium population and diffusion in zirconium

M. E. Foster, X. W. Zhou[a]

Sandia National Laboratories, Livermore, California 94550, USA

ABSTRACT

Tritium population thermodynamics and transport kinetics critically define the tritium storage performance of zirconium tritides that can be used for a variety of nuclear applications including tritium-producing burnable absorber rods. Both thermodynamic and kinetic properties can be sensitive to grain sizes of materials and can be significantly altered by irradiated defects during operation under the reactor environments. A thorough experimental characterization of how these properties evolve under different reactor conditions and different initial grain structures is extremely challenging. Here molecular dynamics simulations are used to investigate tritium population and diffusion in zirconium with and without different planar symmetric and asymmetric tilt grain boundaries and irradiated defects. We found that in addition to trapping tritium, the most significant effect of planar grain boundaries is to increase tritium diffusivity on the boundary plane. Furthermore, fine grain structures are found to mitigate the change of tritium diffusivity due to irradiated point defects as these point defects are likely to migrate to and sink at grain boundaries.

Keywords: Hydrogen isotopes; zirconium; diffusion; molecular dynamics; radiation effects

1. Introduction

Zirconium (Zr) alloys have many important nuclear applications. For example, zirconium can be used to safely store radioactive tritium and has a high storage capacity. This is because Zr can easily hydrogenated, to the fully hydrogenated ε-ZrH_2 phase, which has a strong formation energy of < -0.65 eV/atom [1,2]. This unique property has enabled zirconium tritides to be used as a tritium getter in tritium-producing burnable absorber rods (TPBAR) [3]. For this application, the relative permeability of tritium through zirconium and zirconium tritide phases is the key property

[a] Corresponding author. E-mail address: xzhou@sandia.gov (X. W. Zhou)

because it critically impacts the gettering performance and the safety of the environment. Permeability is the product of solubility and diffusivity so that tritium population thermodynamics and transport kinetics are important. Thermodynamic and kinetic properties are likely to significantly change under reactor conditions due to both phase transformation and formation of irradiated defects such as vacancies (Vac) and self-interstitial atoms (SIA) [4]. These are further influenced by grain structures of materials. A thorough experimental characterization of evolving properties for a variety of microstructures is challenging especially when radioactive species (e.g., tritium) are also involved. Density-functional theory (DFT) calculations have been used to calculate energetics (including diffusion energy barriers of hydrogen isotopes) in various zirconium [5,6,7,8] and zirconium hydride phases [9,10,11,12,13,14] assuming predesignated configurations. Without the constraint to predesignated configurations, molecular dynamics (MD) simulations have been successfully applied to study the radiation effect on tritium population and diffusion in both single crystalline zirconium [15,16] and single crystalline zirconium tritides [17]. These MD simulations have not accounted for microstructures of materials due primarily to grain boundaries (GBs). Grain boundaries can have important effects. First, tritium diffusivities along grain boundaries and in bulk can be significantly different. Second, grain boundaries can be sinks for irradiated point defects and thereby modulate the irradiation effects. Third, grain boundaries can trap tritium and change the tritium population thermodynamics, which appears to comply with the experimental observation that hydrides preferentially form at grain boundaries [18]. It can also be envisioned that the initial saturation of tritium at defects (such as vacancies, dislocations, and grain boundaries) may create an apparent incubation time for tritium release. These effects must be understood to better evaluate and optimize TPBAR performance.

In this paper, we apply MD simulations to study grain boundary and radiation effects on tritium population and diffusion in the hexagonal close packed (HCP) α-Zr. To enable detailed understanding of mechanisms, we focus on designated planar grain boundaries using bicrystal configurations. Numerous symmetric tilt and asymmetric tilt grain boundaries commonly considered for HCP materials [19,20,21] are chosen for the study. Simulations are performed for a variety of configurations with and without grain boundaries, and with and without irradiated point defects (Vac and SIA).

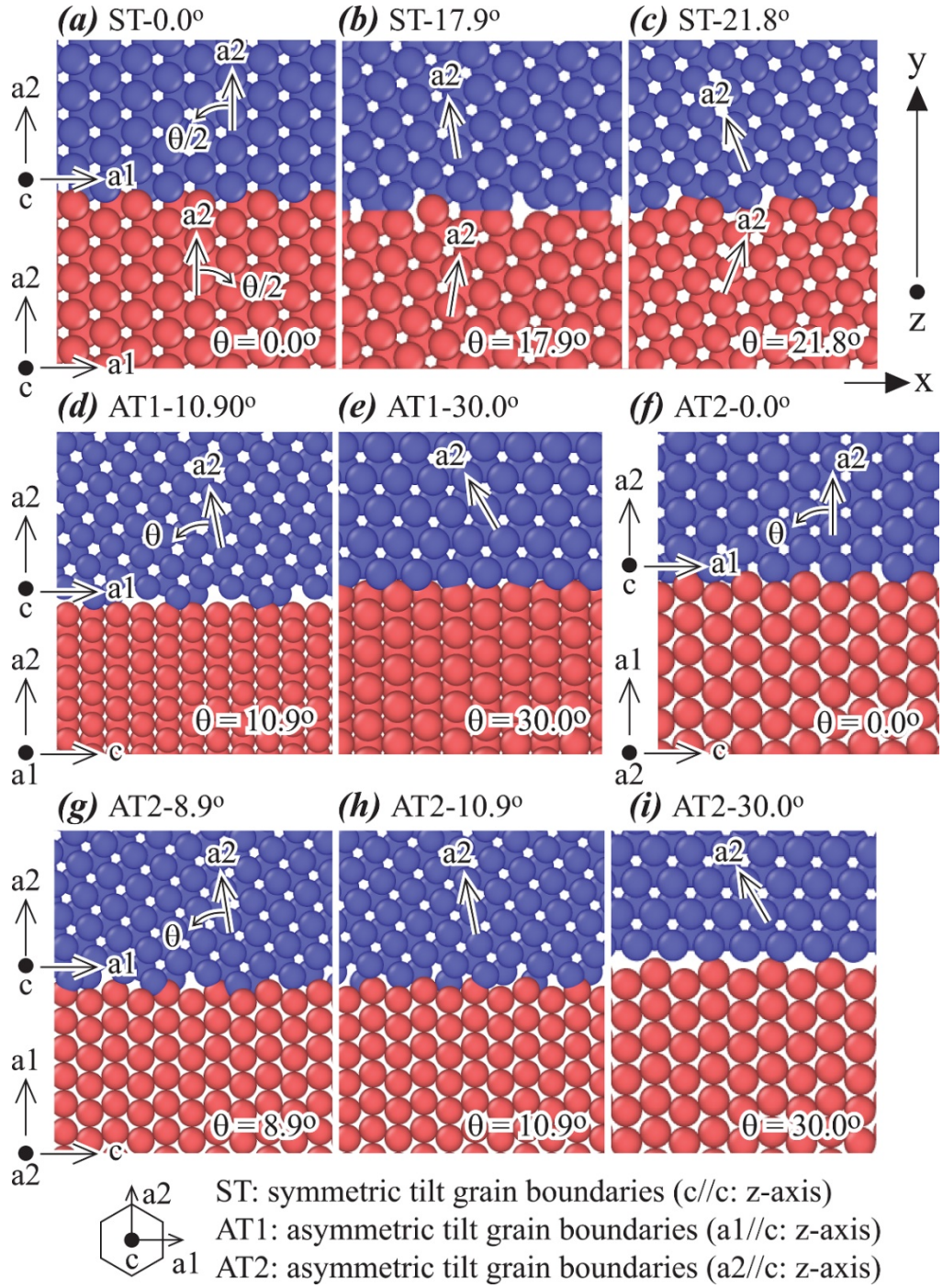

Fig. 1. Illustration of all the nine grain boundaries studied in the present work: (a) ST-0.0° (bulk α-Zr) , (b) ST-17.9°, (c) ST-21.8°, (d) AT1-10.9°, (e) AT1-30.0°, (f) AT2-0.0°, (g) AT2-8.9°, (h) AT2-10.9°, and (g) AT2-30.0°. The Zr atoms are shown in blue and red to illustrate the two grains.

2. Grain geometries

We study nine selected grain boundaries, illustrated in Fig. 1, where red and blue colors

represent grains 1 and 2 respectively. These boundaries span systematically both symmetric and asymmetric tilt grain boundaries commonly observed in α-Zr [19]. Using the three orthogonal axes a1, a2, and c for an HCP unit cell illustrated in the inlet, the un-tilted symmetric tilt (ST) grain boundary shown in Fig. 1(a) satisfies $a1_{grain1}$ // $a1_{grain2}$, $a2_{grain1}$ // $a2_{grain2}$, c_{grain1} // c_{grain2}. This is notated as a ST-0.0° structure which happens to be equivalent to a single crystal without any grain boundary (bulk α-Zr). To create a symmetric tilt angle θ, grain 1 is tilted clockwise and grain 2 is tilted anticlockwise by the same angle θ/2. The corresponding grain boundary is notated as ST-θ and Figs. 1(b) and 1(c) correspond to two such boundaries with θ = 17.9° and 21.8° respectively. Two types of asymmetric tilt grain boundaries are considered. In the first type (AT1), the un-tilted boundary satisfies c_{grain1} // $a1_{grain2}$, $a2_{grain1}$ // $a2_{grain2}$, $a1_{grain1}$ // c_{grain2}. To introduce an asymmetric tilt angle θ, grain 2 is tilted anticlockwise by an angle θ. The corresponding grain boundary is notated as AT1-θ and Figs. 1(d) and 1(e) correspond to two such boundaries with θ = 10.9° and 30.0° respectively. In the second type (AT2), the un-tilted boundary satisfies c_{grain1} // $a1_{grain2}$, $a1_{grain1}$ // $a2_{grain2}$, $a2_{grain1}$ // c_{grain2}. To introduce an asymmetric tilt angle θ, grain 2 is again tilted anticlockwise by an angle θ. The corresponding grain boundary is notated as AT2-θ and Figs. 1(f) - 1(i) correspond to four such boundaries with θ = 0.0°, 8.9°, 10.9° and 30.0° respectively. Note that the tilt angles were selected to closely match the periodic lengths of the two grains on the grain boundary plane. Other tilt angles can also be studied, but the system dimensions may need to be significantly increased to maintain an acceptable periodic length mismatch.

To create a tritium content, the corresponding number of tritium atoms are randomly added into the tetrahedral interstitial sites. To create a SIA content, the corresponding number of zirconium atoms are randomly added to the octahedral interstitial sites. To create a Vac content, the corresponding number of zirconium atoms are randomly removed. Periodic boundary conditions are used. Given the orientation geometries shown in Fig. 1, the system sizes are chosen to ensure that the lattice strain between the two grains is $|\varepsilon| < 2\%$ in any direction. Our system sizes, therefore, vary significantly from 1616 to 3482 Zr atoms. After the tilt grain boundary is created, grain 2 is shifted with respect to grain 1 in the two directions parallel to the grain boundary until a minimum energy at 0 K location is found. This minimum energy configuration is used as the starting configuration for all studies relevant to the GB. Note that the use of small systems only specifies a high relative volume fraction of gain boundary vs. bulk, and it should not impact the

diffusion behavior near grain boundary and in bulk.

3. Simulation methodology

Our simulations were performed with the MD code LAMMPS [22,23,24] under a zero pressure NPT (number of atoms, pressure, and temperature are held constant) ensemble for a total simulated time of 100 ns at a time step size of 0.5 fs. The diffusion analysis was performed on the last 50 ns, allowing ample time for the system to reach equilibrium. The embedded atom method potential developed by Wimmer et al. [25] was used to define interatomic forces. The statistically averaged MD approach based on mean square displacement of tritium as a function of time [26,27,28,29] was used to calculate tritium diffusivities in a 400 - 700 K temperature range. Once diffusivities at different temperatures are known, the diffusion energy barriers and pre-exponential factors can be derived from Arrhenius equation. All simulations were performed at relatively high temperatures to ensure sufficient displacement of tritium atoms. Since only high temperatures are considered, it is assumed that isotope effects are due primarily to atomic mass [30,31]. Note that the simulation results can be easily used to derive 1D diffusivities in arbitrary direction and 2D diffusivities on arbitrary plane. This is because MD simulations essentially determine displacement vector (Δx_i, Δy_i, Δz_i) of all the N_t tritium atoms i = 1, 2, …, N_t as a function of time. The displacement along any direction λ can then be calculated as $d_{\lambda,i} = \cos\alpha\Delta x_i + \cos\beta\Delta y_i + \cos\gamma\Delta z_i$, where α, β, γ are angles between λ and x, y, z axes respectively. The square displacement $d_{\lambda,i}^2$ can then be used to calculate the 1D diffusivities along λ [26,27,28,29]. Similarly, the square displacement on any plane p normal to λ can be calculated as $d_{p,i}^2 = \Delta x_i^2 + \Delta y_i^2 + \Delta z_i^2 - d_{\lambda,i}^2$, which then allows the calculation of the 2D diffusivities on any plane [26,27,28,29]. Through analyses of diffusivities along different directions based on our MD results, we confirm that in the α-Zr, tritium diffusivities on the a1-a2 plane are isotropic, but are lower than diffusivities along c, consistent with the literature DFT based kinetic Monte Carlo calculations [32]. For all the nine structures shown in Fig. 1, diffusion normal to the grain boundary (i.e., along the y-axis) always occur on the a1-a2 plane in the bulk of both grains 1 and 2.

4. Results and discussion

4.1. Tritium trapping by grain boundaries

Tritium trapping by grain boundaries is first explored on systems containing 1% tritium. 1% is appropriate because the system contains a sufficient number of tritium atoms to reduce the statistical errors of the average behavior while at the same time tritium-tritium interactions are not extensive, therefore, closely represents a dilute solution. To this end, time-averaged tritium concentration is calculated as a function of position along the direction normal to the grain boundaries. This is achieved by binning the tritium concentration along the direction normal to the grain boundary. The concentration in each bin is calculated for each time step and averaged over the last 50 ns of the simulation. Note that for our simulated total time and time step, time-averaging means averaging over 10^8 configurations. The concentration thus obtained is further averaged over eight GBs: ST-17.9°, ST-21.8°, AT1-10.9°, AT1-30.0°, AT2-0.0°, AT2-8.9°, AT2-10.9°, and AT2-30.0°. This average is to some extent equivalent to modeling a polycrystalline material where a variety of grain boundaries co-exist; moreover, polycrystalline materials are more experimentally relevant. The results for the defect-free systems (i.e., no SIA and Vac) obtained at 550 K are shown in Fig. 2(a). This figure clearly illustrates that tritium concentrates at GBs; the concentration is found to be approximately three times greater than in bulk regions.

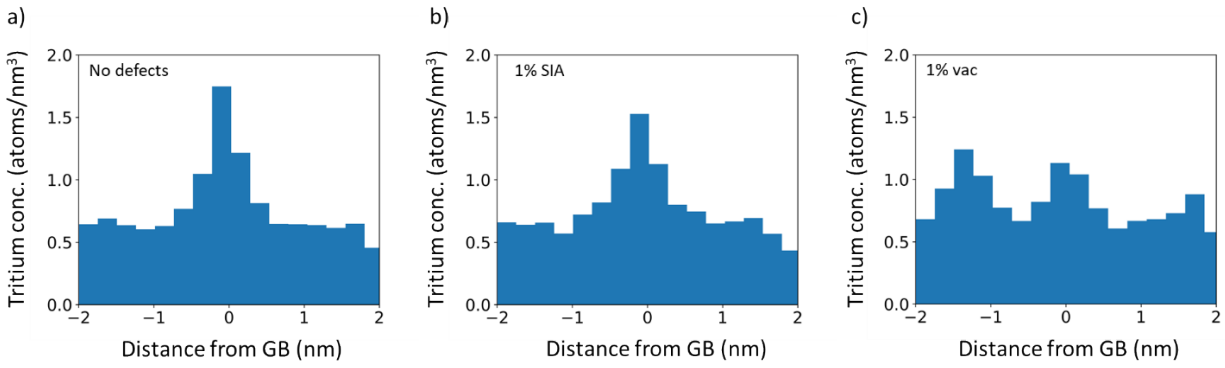

Fig. 2. The time-averaged tritium concentration along the direction normal to the grain boundaries with (a) 1% tritium, 0% SIA, 0% Vac, (b) 1% tritium, 1% SIA, 0% Vac, and (c) 1% tritium, 0% SIA, 1% Vac. These figures were generated from simulations performed at 550 K.

The same analysis was performed on systems containing 1% SIA or Vac, in addition to the 1% tritium. Fig. 2(b) shows the results with 1% SIA; the result is like the case with no defects. This suggests that SIA do not attract tritium; this conclusion is consistent with a previous study of tritium diffusion in α-Zr [15]. We also find that SIA tend to migrate and vanish at grain boundaries; this is another reason why the tritium concentration profile is like the no defect case. In the case

where 1% Vac are introduced, only a slight increase in tritium is observed at the grain boundaries as shown in Fig. 2(c). This is because interstitial tritium atoms get trapped and cluster in the vacancies; once this occurs, the clusters can become immobile (at least within our 100 ns simulations). This is the reason why elevated concentrations are observed, in Fig. 2(c), in regions away from the GBs. As was the case for SIA, Vac can also migrate and vanish at grain boundaries; however, the migration of Vac is slower and can diminishes once occupied by tritium. These results indicate that tritium is attracted to both vacancies and grain boundaries.

Simulations were also performed on systems containing 1% SIA and 1% Vac (Frenkel pairs). Interestingly, we found that a portion of SIA quickly annihilates with Vac while the remaining SIA vanishes at GBs. Hence, the net effect is a reduced Vac concentration without SIA. For clarity, we explore separate SIA and Vac effects in the following.

4.2. Anisotropic bulk diffusion

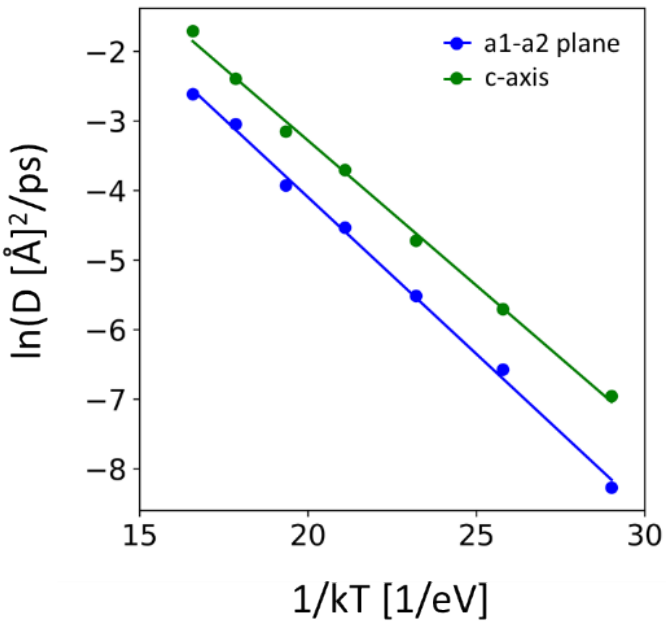

Fig. 3. Arrhenius plots of tritium diffusion along the c-axis and the a1-a2 plane of HCP α-Zr bulk (ST-0.0°). System contains 1% tritium, 0% SIA, 0% Vac.

Discussion of SIA and Vac effects on tritium diffusion in bulk α-Zr have been reported

previously [15]; however, the anisotropic diffusion was not considered. Hence, we calculated Arrhenius plots for tritium diffusion along the c-axis and on the a1-a2 plane in defect-free α-Zr (ST-0.0°); the results are shown in Fig. 3. Diffusivity in the c-direction is faster than on the a1-a2 plane; this agrees with DFT calculations [32] and other literature [32,33] which provides some validation of the potential used in this study.

To understand why diffusion along c-axis is faster than along a1-a2 plane, MD movie with extremely fine time resolution was used to examine diffusion pathways. We found that the c-diffusion is mainly achieved by alternating jumps between tetrahedral-tetrahedral (T-T) interstitial sites and between tetrahedral-octahedral (T-O) interstitial sites, whereas the a1-a2 diffusion is mainly achieved by jumps between T-O interstitial sites. This is consistent with literature [34]. Further, our calculations using nudged elastic band methods [35,36,37] indicated that the diffusion energy barriers for T-T and T-O paths are ~0.2 eV and ~0.6 eV, respectively. The overall diffusion barrier in both c-axis and a1-a2 plane, therefore, is dominated by the ~0.6 eV barrier. However, half of the c-jumps are the lower barrier T-T jumps, and therefore the c-diffusion appears to have a higher pre-exponential factor. These are consistent with Fig. 3 where c-axis and a1-a2 plane seem to have similar energy barrier of ~0.5 eV but c-axis has a higher pre-exponential factor. Experiments also indicated that diffusion of hydrogen along c and a1-a2 has similar energy barrier but c-diffusion is faster [38]. On the other hand, experiments on polycrystalline Zr indicate that the hydrogen diffusion energy barrier falls in the 0.31 – 0.59 eV range [39,40,41,42].

4.3. Tritium diffusion around grain boundaries

The diffusion of tritium in defect-free (i.e., no SIA and Vac) α-Zr with different grain boundaries (see Fig. 1) has been studied. The Arrhenius plots normal and parallel to the various grain boundaries are shown in Figs. 4(a) and 4(b) respectively. The diffusivities normal to GB is independent on the tilting angle because the tilting is always about the c-axis (Fig. 1) and the c-plane has isotropic diffusivities. While diffusivities on GB are anisotropic, averaged values are used because this does not impact our study of defect and grain boundary effects as long as all cases are compared using the same average diffusivities. Further, the linear gray lines in Fig. 4 show the average diffusion in the 8 different GBs; as before, we are mainly concern with the average effect. Fig. 4 also contains the results for bulk α-Zr (ST-0.0°) represented by the linear

blue line. Note, the bulk diffusion curves in each plot are along the same crystallographic directions as for the GBs; this allows for the effect of the GB with respect to bulk diffusion to be observed. Visual comparison indicates that the grain boundaries enhance the diffusivities on the GB planes but does not affect the diffusivities normal to the GBs. These results, along with the tritium concentration profile (Fig. 2), indicate that tritium diffuses to GBs then diffusion is accelerated along the GB plane.

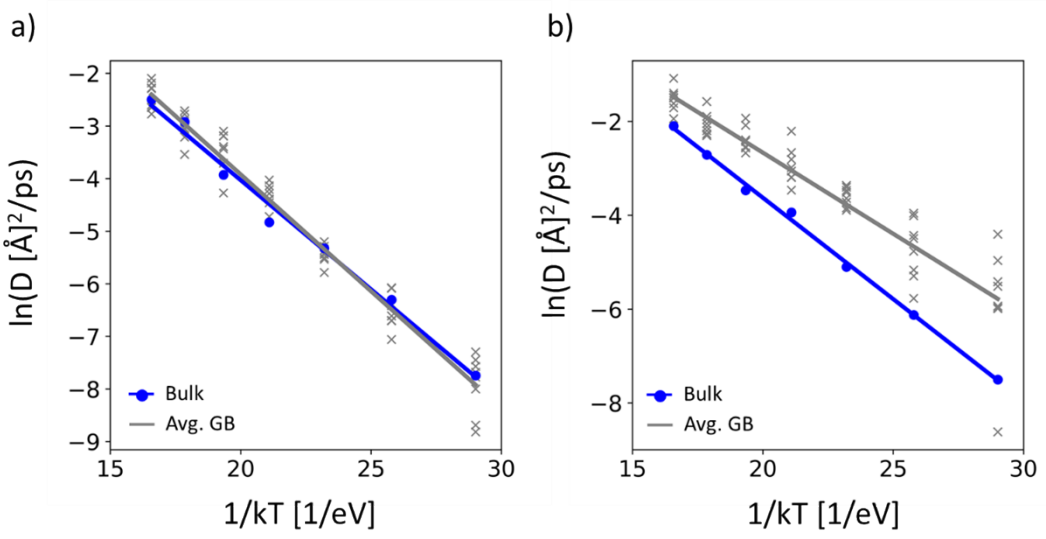

Fig. 4. Arrhenius plots of tritium diffusion in the presence of various grain boundaries: (a) normal to grain boundaries and (b) parallel to grain boundaries. The bulk diffusion values in each plot (blue curves), are along the same crystallographic directions as the GBs (see Fig 1). System contains 1% tritium, 0% SIA, 0% Vac.

To understand why diffusion along grain boundaries is accelerated, an MD movie with a fine time resolution was used to identify a tritium atom jump event on an AT2-30.0° GB at 550 K during 1 ps time span; the atomic configuration is shown in Fig. 5. The figure shows the initial atomic positions plus the final tritium atom location; the initial and final tritium atoms are labeled as I and F. Near the GB, the Zr atoms are distorted so the jump path can no longer be characterized as T-T or T-O jumps. Nudged elastic band calculations indicated that the jump path shown in Fig. 5 has an energy barrier of ~0.1 eV. This lower diffusion barrier, with respect to bulk, is why we observe higher tritium diffusivity along GBs. The distortion is also the likely reason why tritium is observed to segregated at GBs.

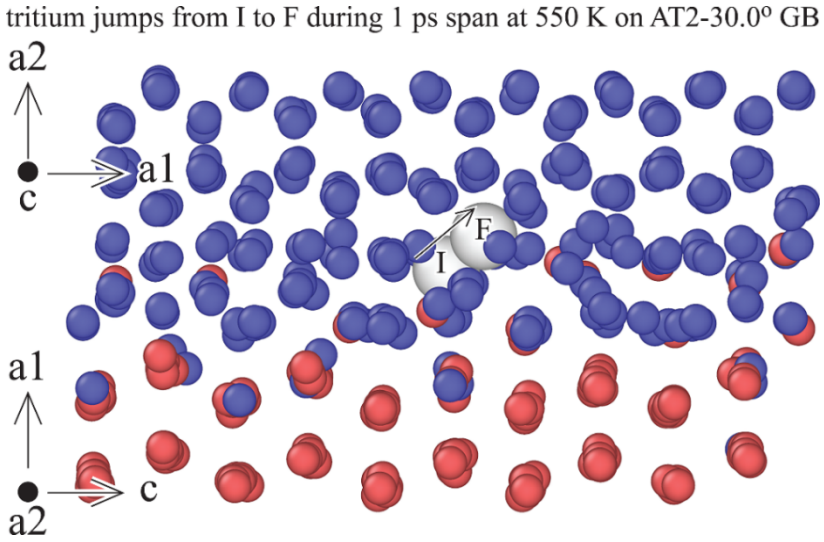

Fig. 5. An initial atomic configuration of an AT2-30.0º GB at 550 K where both initial and final positions of a jumping tritium atom during a 1 ps time span are shown. The Zr atoms are shown in blue and red to illustrate the two grains; the tritium atoms are white, and the atom radius has been enlarged for visualization.

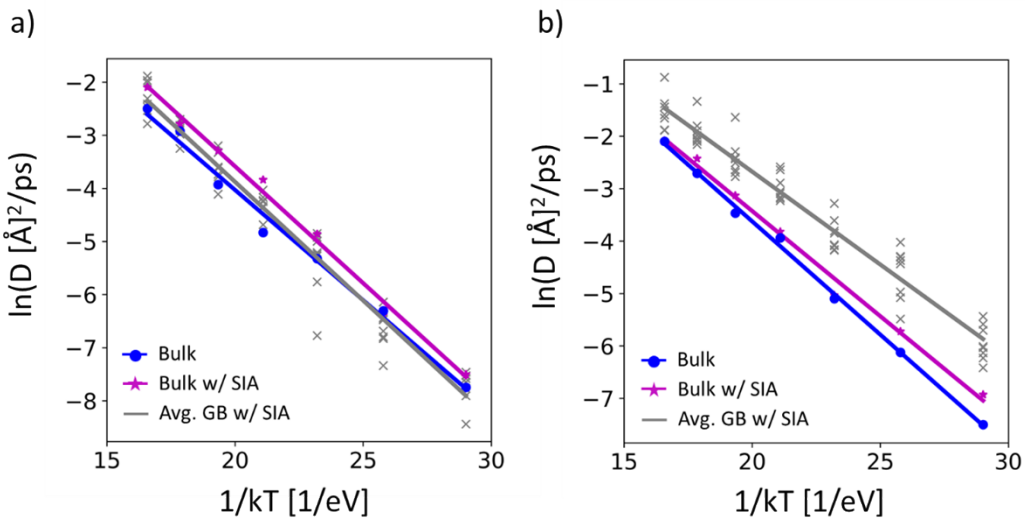

Fig. 6. Arrhenius plots of tritium diffusion in the presence of SIA and various grain boundaries: (a) normal to the grain boundaries and (b) parallel to the grain boundaries. The bulk diffusion values in each plot (blue curves), are along the same crystallographic directions as the GBs (see Fig 1). System contains 1% tritium, 1% SIA, 0% Vac.

We repeated the same analysis with 1% SIA added to the systems (1% tritium, 1% SIA, 0% Vac); the results are shown in Figs. 6(a) and 6(b) for tritium diffusion normal and parallel to the GBs respectively. As is in the case discussed above without SIA, tritium diffusion normal to

the GBs is virtually unchanged and diffusion parallel is increased. These results are consistent with tritium not being attracted to SIA and that SIA vanish at GBs resulting in the same behavior as if SIA were not present. This conclusion is further supported by the Arrhenius plots of tritium with SIA in bulk α-Zr, the magenta line in Fig. 6. Without GBs, 1% SIA slightly increases tritium diffusion due to a lattice expansion effect [15]. Our findings suggest that SIA have little to no effect on tritium diffusion; as was the case without SIA, tritium diffusivity is only effected/increased parallel to the grain boundaries.

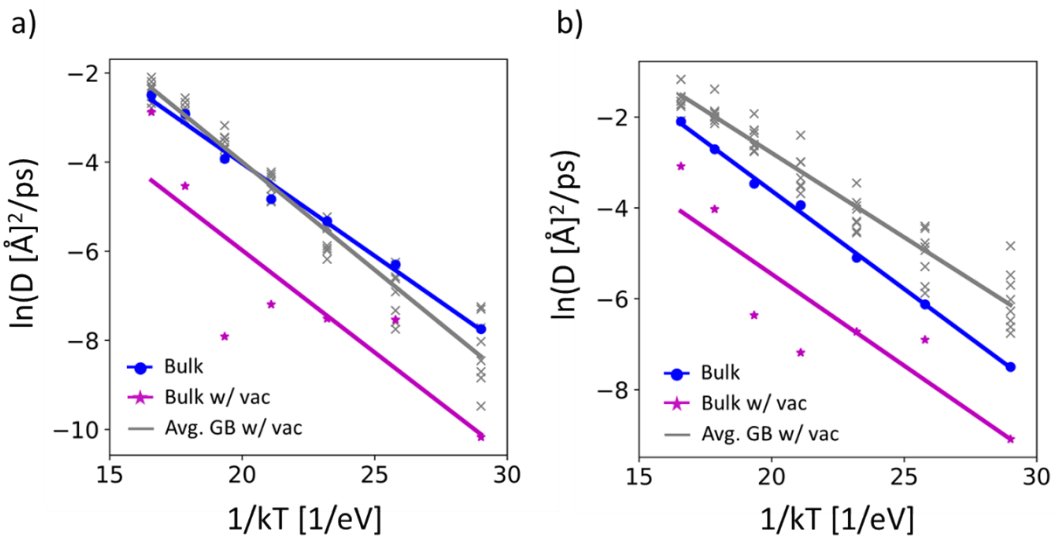

Fig. 7. Arrhenius plots of tritium diffusion in the presence of Vac and various grain boundaries: (a) normal to grain boundaries and (b) parallel to grain boundaries. The bulk diffusion values in each plot (blue curves), are along the same crystallographic directions as the GBs (see Fig 1). System contains 1% tritium, 0% SIA, 1% Vac.

We also perform the same analysis with 1% Vac (1% tritium, 0% SIA, 1% Vac); the results are shown in Figs. 7(a) and 7(b) for tritium diffusion normal and parallel to the GBs respectively. The results are more interesting with vacancies because there are several competing factors: 1) the attraction of tritium to vacancies, 2) the attraction of tritium to grain boundaries and 3) the attraction of Vac to grain boundaries. Arrhenius plots of tritium diffusion in bulk with Vac reveals a significant reduction in diffusion (the magenta line in Fig. 7). This is because tritium is attracted to and cluster in vacancies, causing a decrease in diffusion. The data points (magenta stars) deviate from linear because the trapping rate of tritium depends on the initial proximity to the vacancies; as a result, the diffusion decreases at different times (note that time-averaged MD can mitigate the

effects of initial defect population when the defects are highly mobile). At the end of the 100 ns simulation, all/most of the tritium atoms are trapped in Vac. However, when GBs are present diffusion persists, as evident in Fig. 7. This is because the Vac are also attracted to and vanish at the grain boundaries.

Fig. 8 shows the time-averaged tritium concentration profiles for the different GBs individually with 1% Vac. There it can be seen that in some cases the tritium clusters in bulk regions (e.g. AT2-0.0°) and in other cases tritium makes it to the GB (e.g. AT2-10.9°). In the former, tritium gets trapped in Vac. The latter case occurs because either the tritium reaches the GB before encountering a Vac or the Vac make it to the GB before being occupied by tritium. Fig. 9 visually compares AT2-0.0° with and without Vac; the structures shown are the final MD optimized geometries. It's hard to visually to see regions of increased tritium in these snapshot configurations; however, the time-averaged concentration histogram clearly indicates that the tritium concentration is greater at the GB when no Vac are present but when Vac are introduced, the tritium clusters in regions away from the GB. Note that simulations we performed involve statistical errors which may depend on system size; however, we believe our conclusions are not system size dependent.

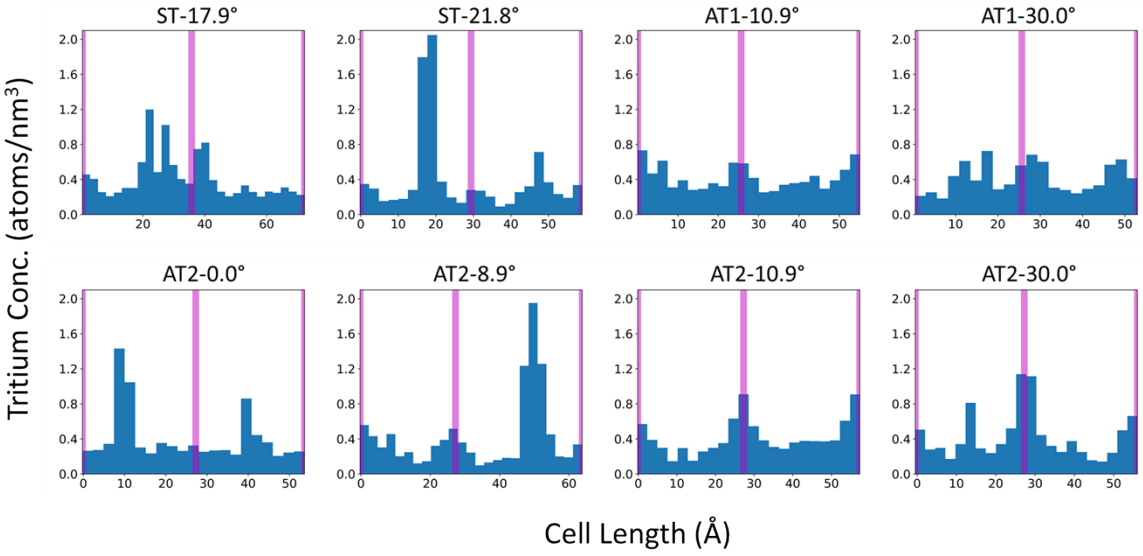

Fig. 8. Time-averaged tritium concentration along the direction normal to the grain boundaries for each system with 1% tritium, 0% SIA, 1% Vac. These figures were generated from simulations performed at 550 K. The magenta line represents the location of the GBs.

Our results indicate that grain boundaries promote the in-plane diffusivities but not significantly the out-plane diffusivities. This is consistent with the GB trapping effect which should only reduce diffusion normal to the GB. The reason that we do not see a significant reduction in diffusivities normal to GB is because the GB thickness is relatively thin compared to the thickness of the internal GB region. However, we only considered infinitely large planar grain boundaries. In realistic polycrystalline materials, there exist junction regions of three or more grain boundaries, and other defects such as dislocation loops. The effects of these defects need to be studied to understand the performance of materials under reactor conditions. We plan to continue to study these effects.

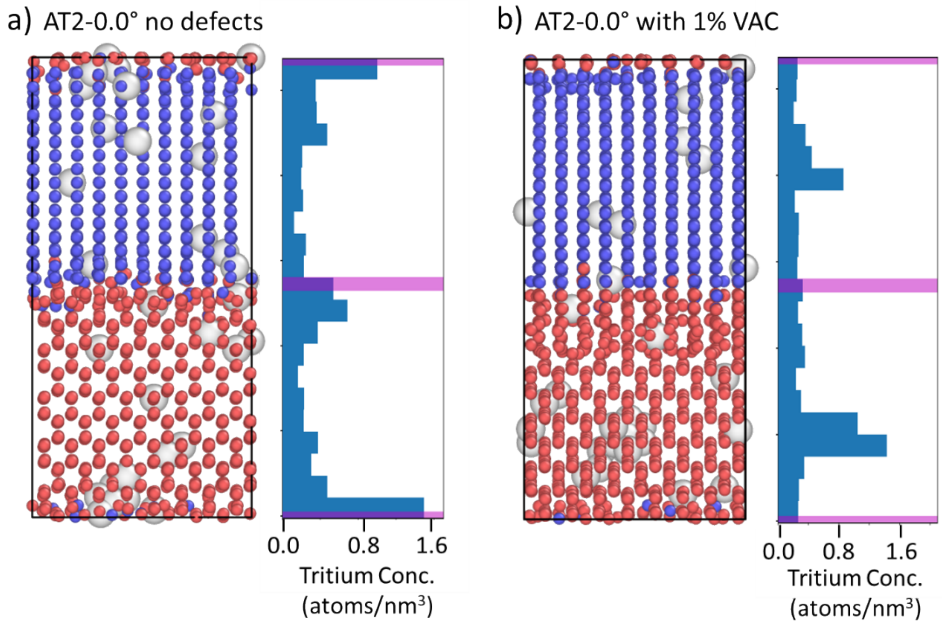

Fig. 9: A schematic showing the optimized geometries after a 100 ns MD simulations at 550 K for AT2-0.0°: (a) with no defects and (b) with 1% Vac. The corresponding time-averaged tritium concentration from the MD simulations are also included. The Zr atoms are shown in blue and red to illustrate the two grains; the tritium atoms are white with the atom radius enlarged for visualization.

5. Conclusions

Our MD simulations of grain boundary and radiation effects on tritium population and diffusion in zirconium have resulted in the following conclusions: 1) Diffusivity of hydrogen

isotopes along the c-axis is higher than on the basal plane of α-Zr. 2) Planar symmetric and asymmetric tilt grain boundaries trap hydrogen isotopes. 3) Diffusion of hydrogen isotopes along grain boundaries is enhanced. 4) SIA slightly increases and Vac significantly decreases diffusivities of hydrogen isotopes in single crystalline Zr (bulk). 5) The effect of SIA and Vac are reduced near grain boundaries because they tend to move to and sink at grain boundaries. This work helps provide a fundamental understanding of how tritium diffuses in Zr which is important for various nuclear applications.

Declaration of Competing Interest

The authors declare that they have no known competing financial interests or personal relationships that could have appeared to influence the work reported in this paper.

Credit author statement

M. E. Foster: Investigation, Writing. **X. W. Zhou:** Conceptualization, Supervision, Writing.

ACKNOWLEDGEMENTS

Sandia National Laboratories is a multi-mission laboratory managed and operated by National Technology and Engineering Solutions of Sandia, LLC., a wholly owned subsidiary of Honeywell International, Inc., for the U.S. Department of Energy's National Nuclear Security Administration (NNSA) under contract DE-NA-0003525. This work describes objective technical results and analysis. Any subjective views or opinions that might be expressed in the paper do not necessarily represent the views of the U.S. Department of Energy or the United States Government. This work is funded by NNSA's Tritium Sustainment Program.

---

1 Y. Zhang, X. – M. Bai, J. Yu, M. R. Tonks, M. J. Noordhoek, and S. R. Phillpot, Homogeneous hydride formation path in α-Zr: Molecular dynamics simulations with the charge-optimized many-body potential, Acta. Mater. 111 (2016) 357.

2 Y. Fukai, The metal-hydrogen system. Springer-Verlag, Berlin, Heidelberg, 1993.

3 K. A. Burns, E. F. Love, and C. K. Thornhill, Description of the tritium-producing burnable absorber rod for the commercial light water reactor TTQP-1-015 Rev 19 (No. PNNL-22086). Pacific Northwest National Lab. (PNNL), Richland, WA (United States), 2012.

4 P. G. Pinchuk, V. N. Bykov, G. A. Birzhevoi, Y. V. Alekseev, A. G. Vakhtin, and V. A. Solov'ev, Nature and thermal stability of radiation-induced defects in zirconium hydride, Soviet Atomic Energy 40 (1976) 356.

5 C. Varvenne, O. Mackain, L. Proville, and E. Clouet, Hydrogen and vacancy clustering in zirconium, Acta Mater. 102 (2016) 56.

6 M. Christensen, W. Wolf, C. Freeman, E. Wimmer, R. B. Adamson, L. Hallstadius, P. E. Cantonwine, and E. V. Mader, H in α-Zr and in zirconium hydrides: solubility, effect on dimensional changes, and the role of defects, J. Phys.: Condens. Matter 27 (2015) 025402.

7 C. I. Maxwell, E. Torres, and J. Pencer, Molecular dynamics study of hydrogen-vacancy interactions in α-zirconium, J. Nucl. Mater. 511 (2018) 341.

8 M. Christensen, W. Wolf, C. Freeman, E. Wimmer, R. B. Adamson, L. Hallstadius, P. E. Cantonwine, and E. V. Mader, Diffusion of point defects, nucleation of dislocation loops, and effect of hydrogen in hcp-Zr: Ab initio and classical simulations, J. Nucl. Mater. 460 (2015) 82.

9 W. Zhu, R. Wang, G. Shu, P. Wu, and H. Xiao, First-principles study of different polymorphs of crystalline zirconium hydride, J. Phys. Chem. C 114 (2010) 22361.

10 Y. Udagawa, M. Yamaguchi, H. Abe, N. Sekimura, and T. Fuketa, Ab initio study on plane defects in zirconium-hydrogen solid solution and zirconium hydride, Acta Mater. 58 (2010 3927).

11 F. Wang, and H. R. Gong, First principles study of various Zr–H phases with low H concentrations, Inter. J. Hydro. Energy 37 (2012) 12393.

12 X. Zhu, D. – Y. Lin, J. Fang, X. – Y. Gao, Y. – F. Zhao, and H. – F. Song, Structure and thermodynamic properties of zirconium hydrides by structure search method and first principles calculations, Comp. Mater. Sci. 150 (2018) 77.

13 I. C. Njifon, and E. Torres, A first principles investigation of the hydrogen-strain synergy on the formation and phase transition of hydrides in zirconium, Acta Mater. 202 (2021) 222.

14 A. V. Yanilkin, Quantum molecular dynamics simulation of hydrogen diffusion in zirconium hydride, Phys. Solid State 56 (2014) 1879.

15 R. Skelton, X. W. Zhou, and R. A. Karnesky, Molecular dynamics studies of lattice defect effects on tritium diffusion in zirconium, J. Nucl. Mater. 555 (2021) 153099.

16 R. Skelton, C. Nowak, X. W. Zhou, and R. A. Karnesky, Tritium segregation to vacancy-type basal dislocation loops in α-Zr from molecular dynamics simulations, J. Appl. Phys. 131 (2022) 125103.

17 P. G. Pinchuk, V. N. Bykov, G. A. Birzhevoi, Y. V. Alekseev, A. G. Vakhtin, and V. A. Solov'ev, Nature and thermal stability of radiation-induced defects in zirconium hydride, Soviet Atomic Energy 40 (1976) 356.

18 N. A. P. K. Kumar, J. A. Szpunar, and Z. He, Preferential precipitation of hydrides in textured zircaloy-4 sheets, J. Nucl. Mater. 403 (2010) 101.

19 Z. Zheng, D. S. Balint, and F. P. E. Dunne, Investigation of slip transfer across HCP grain boundaries with application to cold dwell facet fatigue, Acta Mater. 127 (2017) 43.

20 J. Wang, and I. J. Beyerlein, Atomic structures of symmetric tilt grain boundaries in hexagonal close packed (hcp) crystals, Modelling Simul. Mater. Sci. Eng. 20 (2012) 024002.

21 G. A. Bruggeman, G. H. Bishop, and W. H. Hartt, Coincidence and near-coincidence grain boundaries in hcp metals. In: H. Hu (eds), The nature and behavior of grain boundaries. Springer, New York, 1972.

22 S. Plimpton, Fast parallel algorithms for short-range molecular-dynamics, J. Comp. Phys. 117 (1995) 1.

23 A. P. Thompson, H. M. Aktulga, R. Berger, D. S. Bolintineanu, W. M. Brown, P S. Crozier, P. J. in't Veld, A. Kohlmeyer, S. G. Moore, T. D. Nguyen, R. Shan, M. J. Stevens, J. Tranchida, C. Trott, and S. J. Plimpton, LAMMPS - A flexible simulation tool for particle-based materials modeling at the atomic, meso, and continuum scales, Comp. Phys. Comm. 271 (2022) 108171.

24 LAMMPS download site: lammps.sandia.gov.

25 E. Wimmer, M. Christensen, W. Wolf, W. H. Howland, B. Kammenzind, and R. W. Smith, Hydrogen in zirconium: Atomistic simulations of diffusion and interaction with defects using a new embedded atom method potential, J. Nucl. Mater. 532 (2020) 152055.

26 X. W. Zhou, F. El. Gabaly, V. Stavila, and M. D. Allendorf, Molecular dynamics simulations of hydrogen diffusion in aluminum, J. Phys. Chem. C 120 (2016) 7500.

27 X. W. Zhou, T. W. Heo, B. C. Wood, V. Stavila, S. Kang, and M. D. Allendorf, Temperature- and concentration-dependent hydrogen diffusivity in palladium from statistically-averaged molecular dynamics simulations, Scripta Mater. 149 (2018) 103.

28 X. W. Zhou, R. Dingreville, R. A. Karnesky, Molecular dynamics studies of irradiation effects on hydrogen isotope diffusion through nickel crystals and grain boundaries, Phys. Chem. Chem. Phys. 20 (2018) 520.

29 X. W. Zhou, R. E. Jones, and J. Gruber, Molecular dynamics simulations of substitutional diffusion, Comp. Mater. Sci. 128 (2017) 331.

30 E. Lavert-Ofir, Y.Shagam, A. B. Henson, S. Gersten, J. Kłos, P. S. Zuchowski, J. Narevicius, and E. Narevicius, Observation of the isotope effect in sub-kelvin reactions, Nature Chem. 6 (2014) 332.

31 S. Scheiner, Calculation of isotope effects from first principles, Bio. Bio. Acta, 1458 (2000) 28.

32 Y. Zhang, C. Jiang, and X. Bai, Anisotropic hydrogen diffusion in α-Zr and Zircaloy predicted by accelerated kinetic Monte Carlo simulations, Sci. Rep 7 (2017) 41033.

33 M. Liyanage, R. Miller, and R. K. N. D. Rajapakse, Multiscale approach for determining hydrogen diffusivity in zirconium, Modelling Simul. Mater. Sci. Eng. 26 (2018) 085002.

34 C. Domain, R. Besson, and A. Legris, Atomic-scale ab-initio study of the Zr-H system: I. Bulk properties, Acta. Mater. 50 (2002) 3513.

35 G. Henkelman, and H. Jonsson, Improved tangent estimate in the nudged elastic band method for finding minimum energy paths and saddle points, J. Chem. Phys. 113 (2000) 9978.

36 G. Henkelman, B. P. Uberuaga, and H. Jonsson, A climbing image nudged elastic band method for finding saddle points and minimum energy paths, J. Chem. Phys. 113 (2000) 9901.

37 A. Nakano, A space–time-ensemble parallel nudged elastic band algorithm for molecular kinetics simulation, Comp. Phys. Comm. 178 (2008) 280.

38 J. J. Kearns, Diffusion coefficient of hydrogen in alpha zirconium, zircaloy-2 and zircaloy-4, J. Nucl. Mater. 43 (1972) 330.

39 M. W. Mallett, W. M. Albrecht, Low-pressure solubility and diffusion of hydrogen in zirconium. J. Electrochem. Soc. 104 (1957) 142.

40 C. R. Cupp, P. Flubacher, An autoradiographic technique for the study of tritium in metals and its application to diffusion in zirconium at 149° to 240° C, J. Nucl. Mater. 6 (1962) 213.

41 F. M. Mazzolai, and J. Ryll-Nardzewski, An anelastic study of the diffusion coefficient of hydrogen in α-zirconium, J. Less Comm. Metals 49 (1976) 323.

42 S. Naito, Kinetics of hydrogen absorption by α-zirconium, J. Chem. Phys. 79 (1983) 3113.